ELSEVIER

Eur. J. Med. Chem. 37 (2002) 443–460

EUROPEAN JOURNAL OF MEDICINAL CHEMISTRY

www.elsevier.com/locate/ejmech

Invited review

Physicochemical properties of quinolone antibiotics in various environments

Hyoung-Ryun Park [a], Tae Heung Kim [b], Ki-Min Bark [c,*]

[a] *Department of Chemistry and Institute of Basic Science, Chonnam National University, Kwangju 500-757, South Korea*
[b] *Department of Dermatology, Gyeongsang National University, Chinju 660-701, South Korea*
[c] *Department of Chemical Education and The Research Institute of Natural Sciences, Gyeongsang National University, Chinju 660-701, South Korea*

Received 20 February 2002

Abstract

The progress and photosensitivity of quinolone antibiotics are briefly described. By the photolysis of nalidixic acid, the loss of –COOH group is observed. The photoreaction of fluoroquinolones involves heterolytic C–F bond fragmentation. The protonation and divalent cation complexation equilibria are also examined. The spectroscopic properties of these drugs are intensively investigated in biological mimetic systems such as AOT reverse micelle, and H_2O–CH_3OH and H_2O–CH_3CN mixed solvents. For ofloxacin and norfloxacin, the excited-state intramolecular charge transfer (ICT) is observed. So, fluorescence spectra exhibit reverse solvatochromism in mixed solvents. The change of radiative and non-radiative rate constant can also be explained using this ICT. The influence of dielectric effects of solvent is more significant compared with the specific hydrogen bonding interaction. Theoretical treatments support all of these results.

Keywords: Quinolone antibiotics; Photolysis; Biological mimetic system; Intramolecular charge transfer; Reverse solvatochromism; Radiative and non-radiative rate constant

1. Introduction

Quinolone antibiotics are widely prescribed drugs because of their safety with good tolerance and broad antibacterial spectrum with less resistance [1–4]. In these drugs, there are two types of ring structures, a naphthyridine nucleus, with a nitrogens at position 1 and 8, and a nucleus with only one nitrogen in position 1, referred to as a quinoline nucleus. All compounds, both quinolones and naphthyridones, contain the keto oxygen at C-4 and carboxylic acid side chain at C-3, both of which have now been found to be essential to activity. Moreover, ofloxacin (OFL), norfloxacin (NOR), enoxacin (ENO) etc. have a piperazinyl group at 7-carbon atom. Because these drugs contain carboxyl group, or carboxyl and amine groups, the acid–base behaviour will be influenced by the physicochemical properties of solvent [4,5]. Also, the antibacterial activity is pH-dependent, because these drugs act by inhibition of bacterial DNA gyrase, a process that depends upon both the pH and concentration of the acid [6]. To this effect, the behaviour of quinolones in vivo is significantly influenced by their physicochemical properties, in particular their degree of ionisation [7,8]. It has often been shown that the presence of charged groups is necessary for biological activity and solubility. However, the unionised form has a more favourable partition coefficient toward nonaqueous solvents. Therefore, knowledge of the physical and chemical properties of these drugs such as dissociation constants may be essential for practical purposes and for the interpretation of structure–activity relationships [4,9]. Therefore, quinolone antibiotics having different structures and

Abbreviations: AOT, aerosol-OT, sodium 1,4-bis[2-ethylhexyl] sulfosuccinate; CIP, ciprofloxacin; ENO, enoxacin; FLE, fleroxacin; FLU, flumequine; ICT, intramolecular charge transfer; LOM, lomefloxacin; NAL, nalidixic acid; NOR, norfloxacin; OFL, ofloxacin; OXO, oxolinic acid; PUVA, psoralen plus ultraviolet A; ROS, reactive oxygen species; TICT, twisted intramolecular charge transfer.

* Correspondence and reprints
E-mail address: kiminb@nongae.gsnu.ac.kr (K.-M. Bark).

0223-5234/02/$ - see front matter
PII: S0223-5234(02)01361-2

substituents exhibit different antibacterial responses in various environments [10]. Especially, the two groups of drugs, OFL, NOR, ENO etc., and nalidixic acid (NAL), flumequine (FLU), oxolinic acid (OXO) etc., show completely different antibacterial responses and chemical properties as the physicochemical properties of solvents are changed [5,10–12]. These differences are governed by the presence of piperazinyl group at 7-carbon atom. With OFL and NOR, a pH increment from 5.6 to 8.3, which is the pH range that occurs in urine, progressively increases their activity in nutrient agar. On the other hand, NAL, FLU and OXO become more active in nutrient agar as the pH falls (Fig. 1).

Between quinolone and some divalent cations, 1:1 complexes are formed by ion–dipole interaction using the 4-keto oxygen and the ionised 3-carboxylic acid group [11]. So, when Mg^{2+} is added to an achievable urinary concentration (5.6 mM), the activity of these drugs is reduced at virtually every pH tested, but the antagonistic action of Mg^{2+} on these two groups of drugs, with or without piperazinyl group, does not exhibit similar pH dependence. These observations suggest that there is a major difference between the two groups of drugs, with respect either to their mode of action, or to their mechanism of penetration into bacteria [10]. Furthermore, it is reported that these drugs are able to induce photosensitivity reaction in human skin by sunlight [13]. This phototoxicity will occur in any subject with sufficient cutaneous photosensitiser exposed to enough irradiation of appropriate wavelength, but the mechanism remains still unknown.

It is very important to study the physicochemical properties of these drugs in various environments, especially in vivo because this investigation can provide essential knowledge in our understanding for the mechanism of antibacterial activity and cutaneous photosensitisation. Since it is not easy to study the physicochemical properties of quinolone antibiotics in vivo directly, several investigations have recently been done in biological mimic systems such as AOT reverse micelle or hydro-organic mixed solvents [4,5,9,12,14–16].

Surfactant aggregates in nonpolar solvents assemble to form reverse micelle, aggregations in which the polar heads of the amphiphiles cluster to form a micellar core and the hydrophobic tails extend into the bulk solvent. Among all the possible systems, the Aerosol-OT (sodium 1,4-bis[2-ethylhexyl]sulphosuccinate, AOT) in alkanes (e.g. *n*-heptane or isooctane) has been the most widely investigated for its ability to form reverse micellar aggregates in nonpolar solvents and to solubilise and compartmentalise relatively large amounts of water within their central core [5,17–26]. As the molar ratio of water to AOT

$$R = \frac{[\text{water}]}{[\text{AOT}]}$$

increases, the hydrodynamic radius of the spherical aqueous micellar core grows monotonically. The water solubilised in AOT–H_2O–alkane microemulsions, in any respects, is similar to the interfacial water present near the biological membranes or at the protein sur-

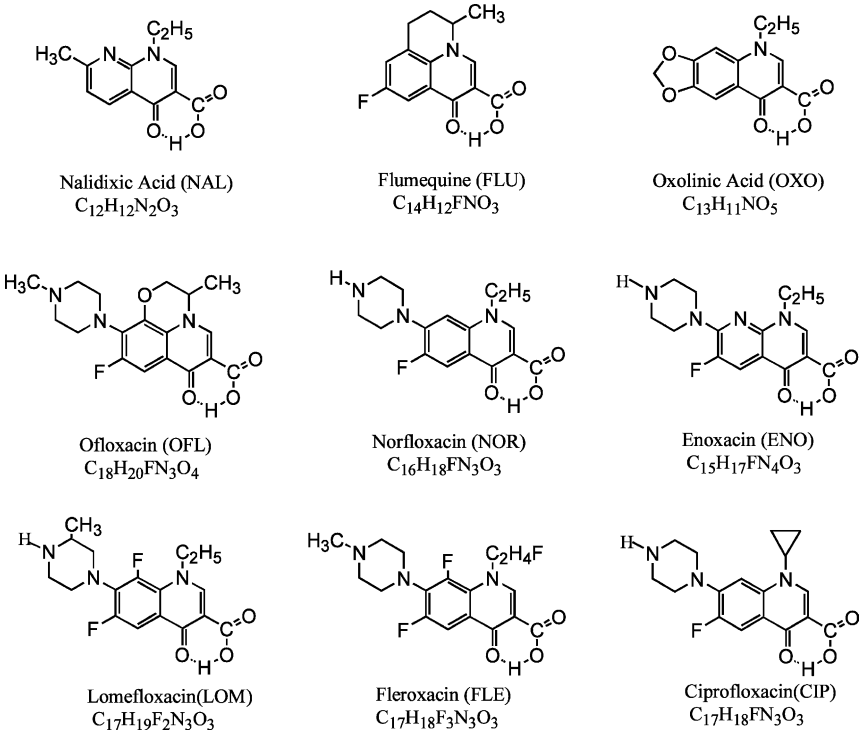

Fig. 1. Chemical structures of selected quinolone antibiotics. The proposed hydrogen-bond is represented by a dotted line.

faces [23,27,28]. So, AOT reverse micelle has been thought to behave as a membrane mimetic system.

Hydro-organic mixtures such as H_2O–CH_3OH and H_2O–CH_3CN have also been found suitable to emulate the biological conditions because they simultaneously show low polarity and a partially aqueous content, always present in biological systems [4,9,12]. In H_2O–CH_3OH and H_2O–CH_3CN mixed solvents, the change of π^* scale, which is an index of solvent dipolarity/polarisability, are similar to each other as the composition of binary mixtures is changed. However, the α scale, which is the solvent hydrogen-bond donor acidity, of water and methanol are similar but this values of water and acetonitrile are quite different.

In this article, we intensively review the physical and chemical properties of some selected quinolone antibiotics, characterised by spectroscopic techniques, in biological mimetic systems. Special attention is given to investigate the question that how strongly the photochemical properties of solutes are influenced by the solvent–solute interactions. Also, it will briefly be described the evolution and development, photosensitivity, and photochemical reactions of these drugs.

2. The progress and photosensitivity of quinolone antibiotics

Quinolone antibiotics are active against a variety of gram-positive and gram-negative bacteria, and they act by the inhibition of DNA gyrase (topoisomerase II), a bacterial enzyme involved in DNA replication, recombination and repair, leading to bacterial cell damage [29]. Compared with other drugs, quinolone antibiotics have a rapid bactericidal effect against most susceptible organisms, that is very important for patients who are seriously ill or for patients with defective or impaired immune system. In addition, they penetrate into tissues and mammalian cells extremely well which enables their widespread use in clinical medicine [1].

Quinolones are originated from antimalarial agent chlorquine, but NAL, the first generation quinolone antibiotics synthesised in 1962, had only modest antibacterial activity against gram-negative species and showed poor oral absorption. Introduction of a piperazinyl side chain at position 7 improved the activity against gram-negative bacteria and increased the penetration into bacterial cell wall [30]. Fluorination at position 6, which was called fluoroquinolone antibiotics, increased their activity against gram-positive bacteria [31]. Modification of molecular structure by substitution of both piperazinyl group and fluorine atom improved their efficiency greatly as shown in the case of NOR, ENO, fleroxacin (FLE), ciprofloxacin (CIP) and OFL. These compounds had broad antibacterial spectrum extending to most gram-positive species but their effect is still inadequate to treat respiratory infections. Recently developed newer generation quinolones are trying to solve these problems by enhancing activity against gram-positive or anaerobic bacteria [1]. They are also active against atypical organisms like mycoplasma, chlamydiae, legionella or some mycobacteria [29].

Drug-induced photosensitivity can be divided into phototoxicity and photoallergy. Phototoxicity is an adverse cutaneous response to the combined actions of a chemical agent such as a drug and a physical agent such as UV radiation. The quinolone antibiotics are one of typical photosensitiser [32]. Phototoxicity owing to these antibiotics was caused by the reactive oxygen species (ROS) [33]. Oxygen-dependant release of ROS induces phototoxic damage on cell surface [34], DNA [35], and lysosome [36]. In an in vivo mouse experiment, phototoxicity increased UVA-induced edema, sunburn cell formation and local suppression of immune response [32]. Increment of prostaglandin E2 production [37] and depletion of Langerhans cells [32] owing to phototoxicity would be responsible for this local immune suppression.

Clinically, phototoxicity shows features of exaggerated sunburn, and long-term intake of a photosensitiser may induce cataract of ocular lens or photo-aging of skin [38]. Phototoxicity, particularly in case of psoralen plus ultraviolet A (PUVA), may increase skin cancers like squamous cell carcinoma and malignant melanoma [39,40]. Quinolone antibiotics were also able to induce photocarcinogenesis like PUVA. Lomefloxacin (LOM) or FLE, which have another fluorine atom at C-8, exhibited increased photocarcinogenic potentials [41,42]. Most quinolones show phototoxicity in various in vitro methods, which examine fluorescence or phototoxic killing of organisms or phototoxic destruction of cells, and in vivo methods, which measure swellings or erythema [32].

Quinolone antibiotics also induce photoallergy, another feature of UV-induced skin lesion. This photoallergy shows features of allergic contact dermatitis like poison ivy in exposed areas. Without UV irradiation, they are usually inert. In the presence of UV light, quinolone antibiotics are activated to bind with skin protein, which becomes complete antigen and induces allergic dermatitis. In contrast to phototoxicity, it is difficult to make an optimal experimental model [43,44].

In structure–activity relationship studies, each positions of molecule are well examined analytically. In photobiologic point of view, position 8 seems very critical in its phototoxicity. Substitution of position 8 with halogens increases phototoxicity [1], but substitution of this position with methoxy group reduces phototoxicity [45].

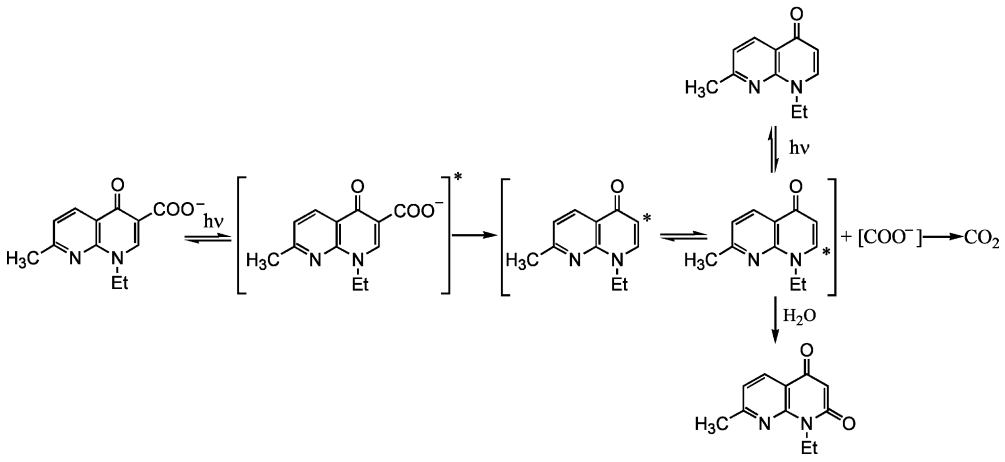

Scheme 1.

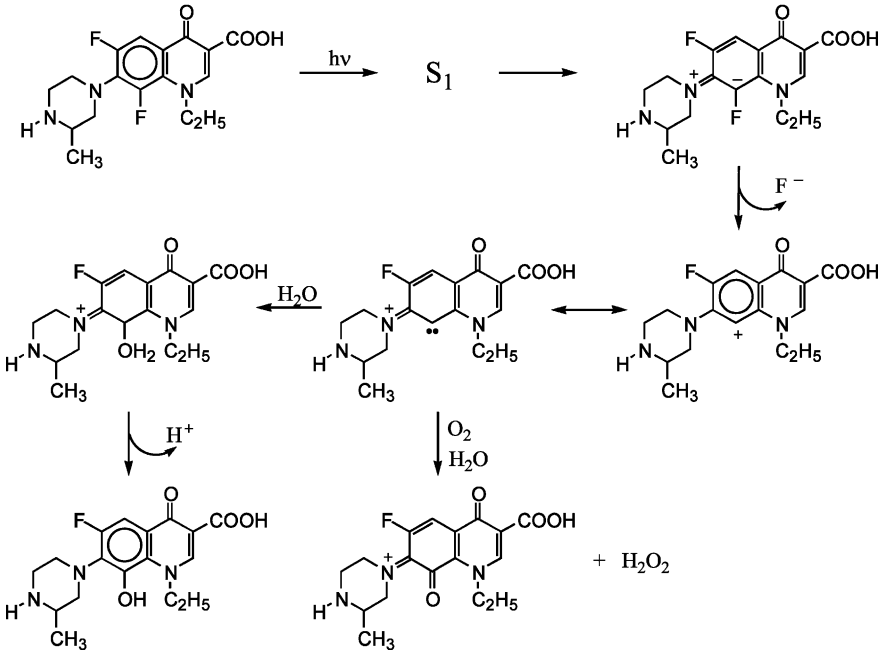

Scheme 2.

3. Photochemical reaction

The study for the photochemical reaction of the quinolone antibiotics is very important to understand the mechanism of antibacterial activity and photosensitivity. However, this area has not been investigated actively. In earlier study on the photolysis of NAL, Detzer et al. have reported that photochemical decomposition of oxygen free NAL in basic solution was undergone to be loss of the –COOH group at position 3 as shown in Scheme 1 [46]. As a result of the decarboxylation, 1-ethyl-1,4-dihydro-7-methyl-4-oxo-1,8-naphthyridine was obtained. Carbon dioxide, ethylamine and 1-ethyl-1,4-dihydro-7-methyl-2,4-dioxo-1,8-naphthyridine were also produced. Fernandez et al. reported that the photolysis of NAL produced the 1-ethyl-1,4-dihydro-7-methyl-4-oxo-1,8-naphthyridine by UV irradiation [47]. They proposed that this photoproducts produced photohaemolysis by oxygen-dependent mechanisms.

In 1997, Martinez et al. reported that the highly effective photolysis { > 320 nm, quantum efficiency (ϕ_{dec}) = 0.98 at pH 7.4} of the LOM and FLE results in the loss of fluorine at position 8 as fluoride ion (see Scheme 2) [48]. The mechanism probably involves aryl-F heterolysis from the S_1 state with the concomitant generation of carbene at C-8. Carbenes are highly reactive chemical species that undergo addition, insertion and abstraction reactions, and can cause DNA cleavage. In contrast, NOR and CIP, which are the

monofluorinated quinolones, do not generate fluoride ion by irradiation. These facts may explain why LOM and FLE are more photomutagenic and photocarcinogenic than fluoroquinolones in which C-8 is either unsubstituted or bears a substituent other than fluorine. Albini et al. have also investigated the photoinduced C–F bond cleavage of some fluoroquinolone antibiotics in water and 0.1 M phosphate buffer [49–53]. All of them undergo heterolytic defluorination, and this appears to be a path for the generation of aryl cations in solution. The quantum efficiency is both structure and medium dependent. Φ_{dec} is close to 0.5 both in water and in 0.1 M phosphate buffer for LOM; 0.01 for ENO and 0.004 for NOR in buffer, but more than an order of magnitude higher in neat water. For 6-fluoro derivatives such as NOR and ENO, this cleavage of the C–F bond gives the corresponding phenols. Insertion of an electron-donating substituent makes defluorination inefficient; thus OFL, an 8-alkoxy derivative, is found to be rather photostable ($\Phi_{dec} = 0.001$) and reacts in part via a process different from defluorination (degradation of the *N*-alkyl side chain) in water. With a 6,8-difluoroderivative, LOM, the reaction is more efficient and selective for position 8. Contrary to the NOR and ENO, Albini et al. suggest that the aryl cation undergoes insertion in the neighbouring *N*-ethyl group rather than solvent addition (a carbene-like chemistry). The efficiency of heterolytic C–F bond fragmentation is determined by the excited-state intramolecular charge transfer (ICT) character, which increases in the series OFL < NOR < ENO < LOM according to the electronegativity of the substituent in position 8, and by the stabilisation of the resulting aryl cation (larger for the 8-cation than for the 6-cation).

In addition to the investigation for the photoproducts, Vermeersch et al. has reported the study of a laser flash photolysis with 355 nm and corresponding photosensitisation of NAL [54]. This photolysis of NAL in the aqueous medium with pH 9.2 leads to the formation of the nalidixate anion triplet state ($^3NAL^-$) with high quantum yield ($\Phi_T \geq 0.6$). Whereas efficient singlet oxygen production ($\Phi_\Delta \approx 0.2$) was demonstrated by Dayhaw-Barker and Truscott [55], the $^3NAL^-$ is also quite reactive with good electron donors such as tryptophan or tyrosine. The nalidixate radical dianion formed during this electron transfer reacts rapidly with oxygen to give the superoxide anion. The strong reactivity of this water soluble photosensitiser with such biologically important substrates may be in fact a determinant in the well-known phototoxicity of NAL in vivo, given its tendency to bind to soluble macromolecules [56]. In 1984, Douglas et al. tested the photosensitisation by NAL and OXO in aqueous solution using 365 nm radiation [57]. However, the quantitative photochemical study, which investigates the reaction pathway based on the product analysis of the quinolone antibiotics, is not much reported yet.

4. Ionisation and complex formation with divalent cations

Quinolone antibiotics have several potentially ionisable functional groups. Because the pK_a of aniline (4.60) and pyridine (5.23) are very small, the nitrogen atoms at position 1, 8 and N-1 of the piperazine ring can hardly exhibit acid–base properties within the pH ranges of pharmaceutical or physiological importance. So, the quinolones such as NAL, FLU and OXO etc. have only one relevant ionisable functional group, the 3-carboxyl group. In contrast, OFL, NOR and ENO etc. have two relevant ionisable functional groups, the 3-carboxyl group and N-4 of the piperazine substituent. In UV absorption spectra, one isosbestic point was observed for NAL, FLU and OXO, but two isosbestic points were exhibited for OFL, NOR, and ENO [11]. The ionisation equilibria of NAL and OFL are presented in Scheme 3.

The ionisation constants of some selected quinolones were obtained recently [11]. The apparent ionisation constants are measured by spectrophotometric method. By potentiometric titration method, one or two ionisa-

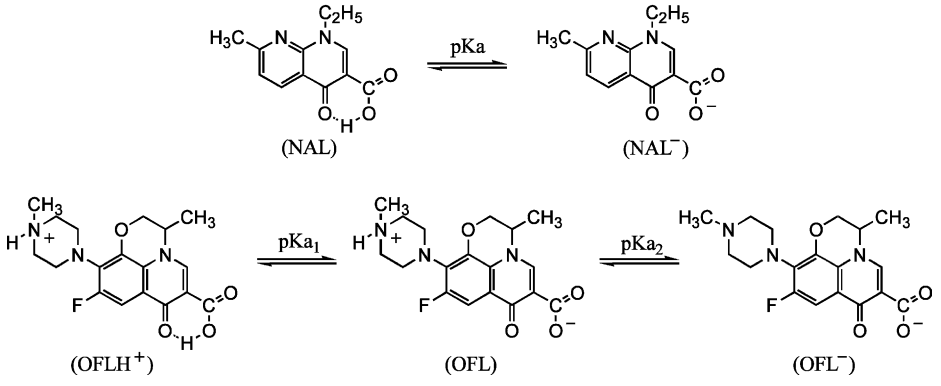

Scheme 3.

Table 1
Ionisation constant of quinolone antibiotics in aqueous solution using both spectrophotometric and potentiometric titration methods

Quinolone antibiotics	Spectrophotometric method pK'_a	Potentiometric titration method		
		pK_{a1}	pK_{a2}	pK_I
NAL	6.33	6.41		6.41
FLU	6.51	6.50		6.50
OXO	6.72	6.61		6.61
OFL	7.18	6.10	8.28	7.19
NOR	7.26	6.23	8.55	7.39
ENO	7.53	6.32	8.62	7.47

pK'_a and pK_I indicate the apparent ionisation constant and isoelectric point, respectively. Uncertainty of all these data is less than 1.5%.

tion constants are observed as shown in Table 1. The ionisation constants of NAL, FLU and OXO measured by two methods are the same within experimental error. Also, the isoelectric points of OFL, NOR and ENO, obtained by averaging the pK_{a1} and pK_{a2}, are the same as the apparent ionisation constants within experimental errors.

The pK_{a1} of these drugs are high about 2 pK units, compared with the structurally related benzoic acid ($pK_a = 4.20$). This result indicates the existence of the intramolecular hydrogen-bond between the proton of the unionised carboxylic acid group and the keto oxygen [11,58–61]. Acidity of the amine group in piperazine substituent of OFL, NOR, and ENO is still greater than that of piperazine ($pK_a = 9.71$). If the proton can move from the carboxylic group to the N-4 in the piperazinyl group via hydrogen bonding of water molecules, the ionisation of the amine group may arise partly from the combination with the proton produced by ionisation of the carboxyl group instead of hydrolysis of water. This proton transfer may contribute to the increase in acidity of the amine group in this substituent [11].

The complex formation between quinolone antibiotics and divalent cations plays an important biological role. The ability of these drugs to interact with some cellular components is mediated by this complexation [2]. Several studies have shown that a DNA gyrase cannot bind quinolones in the absence of DNA and the amount of quinolone bound to DNA is modulated by the Mg^{2+} concentration [2,4,10,62]. The photocarcinogenic potential of some quinolones could be related to their ability to interact with DNA [2,58]. Since it has been reported that many enzymes having nucleic acids as substrates or templates contain a nonmagnesium divalent cation, the complex formation with divalent cations of transition metals would be of far greater interest and possible importance [63–68].

It was recently reported that the formation constants (K_f) with some divalent cations were measured for OFL, NOR and FLU in pH 7.5 as shown in Table 2 [11]. For cations belonging to the alkaline earth metals, the K_f values decrease going down a group in the periodic table owing to the increase of cationic radii. In transition metals, the K_f values of Mn^{2+} and Zn^{2+} are relatively small compared with those of Ni^{2+} and Co^{2+}. Besides the ion–dipole interaction, additional weak orbital–orbital interactions may exist between d orbital of $Ni^{2+}(d^8)$ or $Co^{2+}(d^7)$, and ligand. However, this orbital–orbital interaction will be negligible for Mn^{2+} and Zn^{2+} because the d orbital of Mn^{2+} is half filled and that of Zn^{2+} is fully filled. Therefore, Ni^{2+} and Co^{2+} form more stable complexes with these drugs. For all the ions tested, FLU has somewhat larger K_f values because the molecular size of FLU is the smallest. Furthermore, the positive charge on the zwitterion of OFL and NOR makes it harder for the metal cations to approach the binding site. The composition of the complex is 1:1 for all cations [11,69]. The N-4 in the piperazinyl group of OFL and NOR may also participate in the complexation. However, it is likely that the piperazinyl nitrogen serves to stabilise the complex slightly but can not be considered the primary binding site [11,70–72].

Table 2
Apparent complex formation constants of OFL, NOR and FLU with divalent cations

Cation	log K_f [a]		
	OFL	NOR	FLU
Mg^{2+}	2.9	2.9	3.2
Ca^{2+}	2.3	2.2	3.1
Sr^{2+}	1.1	1.2	1.3
Ba^{2+}	1.1	1.1	1.1
Mn^{2+}	3.3	3.4	3.6
Zn^{2+}	3.9	3.9	4.0
Co^{2+}	4.2	4.4	4.6
Ni^{2+}	4.3	4.4	4.5

[a] Uncertainty is less than 4%.

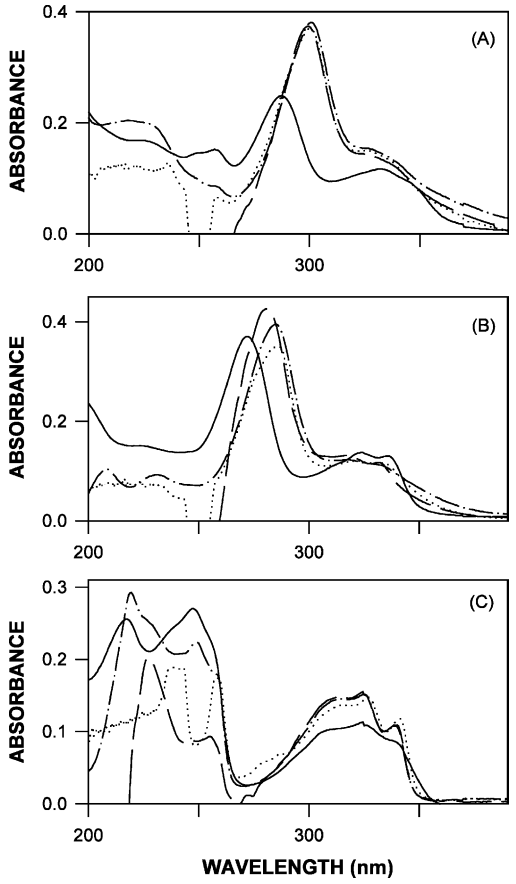

Fig. 2. Absorption spectra for 1×10^{-5} M antibiotics in water (—), methanol (– – –), acetonitrile (–·–·), and chloroform (·····). (A) OFL, (B) NOR, (C) FLU.

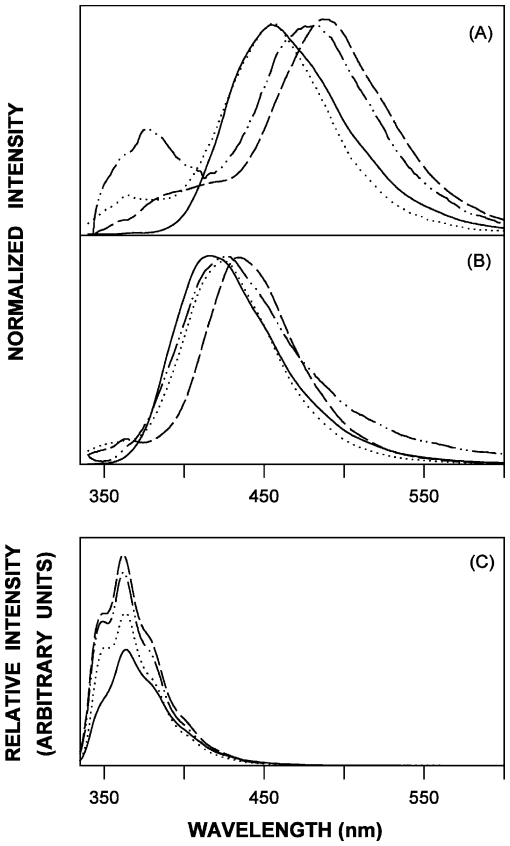

Fig. 3. Steady-state fluorescence emission spectra for 7×10^{-6} M antibiotics in water (—), methanol (– – –), acetonitrile (–·–·), and chloroform (·····). $\lambda_{ex} = 325$ nm; $T = 25.0$ °C. (A) OFL, (B) NOR, (C) FLU.

5. Spectroscopic properties in various environments

5.1. Absorption and fluorescence spectra

To study the spectroscopic properties of quinolone antibiotics, OFL, NOR and FLU, were selected as a model compounds [5,12]. The UV absorption spectra of these molecules in various solvents are shown in Fig. 2 [5]. In aqueous solution, the absorption spectrum of OFL and NOR contain two major bands. In organic solvents, the strong band shifts toward the long wavelength side by ~15 nm. Fig. 3 shows the steady-state emission spectra and Table 3 lists the fluorescence spectral data for these compounds in various solvents [5]. In aqueous solution, the emission spectra of OFL and NOR are strong, broad structureless band with large Stokes' shift. In organic solvents, the emission intensities of OFL and NOR are very weak, the lifetimes become long and another small band appears in short wavelength region (350–400 nm). Moreover, the red shift of main emission band is observed in CH_3OH and CH_3CN compared with that in aqueous solution. The absorption and emission spectra of OFL and NOR in organic solvents have roughly mirror image relation-

Table 3
Fluorescence emission centres of gravity (E), Stokes' shifts ($\Delta\nu$), fluorescence quantum yields (Φ_F) and fluorescence lifetimes (τ) of antibiotics in various solvents

Solvent	E (nm) [a]	$\Delta\nu$ (cm^{-1}) [a]	Φ_F	τ (ns) [d]
OFL				
H_2O	475	8984	0.199 [b]	5.86
CH_3OH	482	9931	0.006 [c]	12.5
CH_3CN	492	10 276	0.002 [c]	13.7
$CHCl_3$	455	9535	0.004 [c]	14.2
NOR				
H_2O	436	7160	0.160 [b]	2.30
CH_3OH	448	7901	0.020 [c]	2.56
CH_3CN	440	7576	0.002 [c]	3.05
$CHCl_3$	419	7409	0.008 [c]	3.27
FLU				
H_2O	375	3987	0.034 [b]	0.73
CH_3OH	371	3761	0.034 [b]	0.82
CH_3CN	370	3595	0.025 [b]	0.76
$CHCl_3$	372	3652	0.036 [b]	0.71

[a] Uncertainty is ≤3%.
[b] Uncertainty is ≤5%.
[c] Uncertainty is ≤25% owing to very low fluorescence intensity.
[d] Uncertainty is ≤10%.

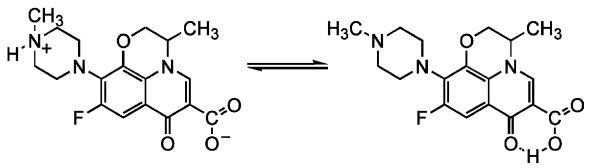

Scheme 4.

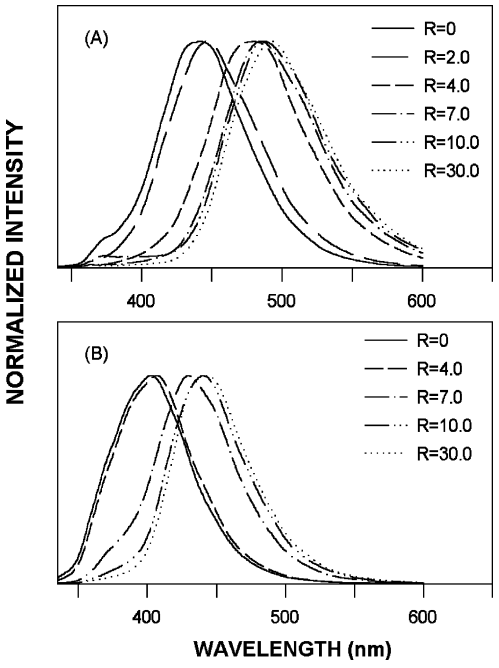

Fig. 4. Steady-state fluorescence emission spectra for 7×10^{-6} M antibiotics in AOT–H_2O–heptane reverse micelle as a function of added water. Actual water added (R) is shown in the inset of the Figure. $\lambda_{ex} = 325$ nm; $T = 25.0$ °C. (A) OFL, (B) NOR.

ships, especially for OFL. Such observations indicate that the geometry change upon excitation is small in organic solvents.

For all three molecules, the changes of dipole moment upon excitation are small in gas phase [5]. In aqueous phase, this dipole moment changes of OFL and NOR are very large. These experimental and theoretical calculations suggest that OFL and NOR will exist mainly in neutral zwitterionic forms in water but these molecules exist mainly in molecular forms in organic solvents [4,5,9,12]. Therefore, the equilibrium shown in Scheme 4 can be proposed for these molecules. Because the internal conversion rate of $S_1 \rightarrow S_o$ for OFL and NOR will be very fast in organic solvents owing to the similar geometrical structures and dipole moments between these states, the fluorescence quantum yield becomes very low [73]. Furthermore, the lifetimes of OFL and NOR in organic solvent are longer than those in water. However, the fluorescence properties of FLU are relatively insensitive to the solvent properties as shown in Table 3.

Fig. 4 shows the steady-state fluorescence emission spectra of OFL and NOR dissolved in AOT reverse micelles as a function of added water [5]. When the R value increases, the large red shift of emission bands is observed. Table 4 lists the fluorescence spectral data of these molecules in AOT micelle. The lifetime of OFL and NOR increases gradually as the water concentration increases. Also, as shown in Fig. 5, the position of the emission band of OFL (or NOR) shifts toward the long wavelength side with increasing temperature when the water content is small ($R < 3$). As the more water is incorporated into the micelle, this red shift decreases and disappears eventually at $R > 10$.

In AOT reverse micelles, quinolones will be present mainly in anionic form, since it is known that the micelle core is normally basic [24,74]. Because quinolones are insoluble in n-heptane, it is confident that this molecule does not reside outside the micelles or even in the middle of the alkyl tails of the surfactants. According to the previous study for AOT micelle, it can be suggested that quinolone molecules interact strongly with the micellar interface near the AOT headgroup, do not necessarily reside in a well-defined water

Table 4
The fluorescence centres of gravity (E), Stokes' shifts ($\Delta\nu$) and apparent fluorescence lifetimes (τ) of antibiotics in AOT reverse micelle as a function of added water

R	OFL			NOR			FLU		
	E [a] (cm^{-1})	$\Delta\nu$ [a] (cm^{-1})	τ [b] (ns)	E [a] (cm^{-1})	$\Delta\nu$ [a] (cm^{-1})	τ [b] (ns)	E [a] (cm^{-1})	$\Delta\nu$ [a] (cm^{-1})	τ [b] (ns)
0	22 356	8461	3.32	24 552	5523	2.01	27 005	3812	0.88
2	21 925	8892	3.26	24 504	5571	2.39	26 882	3935	1.01
4	20 572	10 056	4.30	24 372	5658	3.04	26 925	3892	1.02
7	20 149	10 479	5.16	22 826	7249	3.33	26 961	3856	1.04
10	20 105	10 523	5.49	22 277	7798	3.36	26 940	3877	1.09
15	19 944	10 684	5.56	22 193	7882	3.17	26 896	3921	1.01
30	19 885	10 743	5.62	22 090	7985	3.12	26 954	3863	1.13

$T = 25$ °C.
[a] Uncertainty is $\leq 3\%$.
[b] Uncertainty is $\leq 10\%$. Lifetimes are measured at emission maximum.

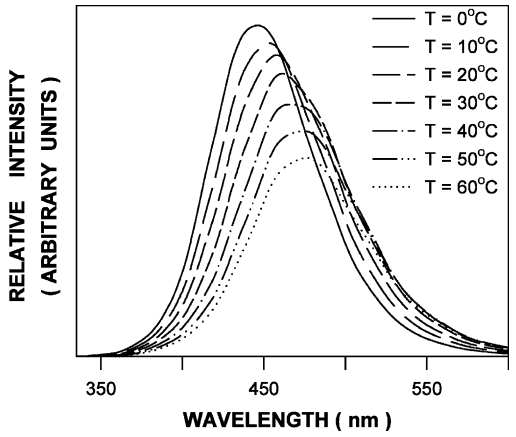

Fig. 5. Steady-state fluorescence emission spectra for 7×10^{-6} M OFL in AOT–H_2O–heptane reverse micelle as a function of temperature. Actual temperatures are shown in the inset of the Figure. $\lambda_{ex} = 325$ nm; added water content, $R = 0$.

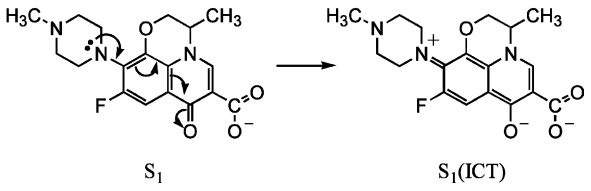

Scheme 5.

pool, and rotate much more slowly in the interior of AOT micelle regardless of the water concentration [22,24,75,76].

5.2. Excited-state intramolecular charge transfer

The OFL and NOR have two electron releasing nitrogen atoms; the one is the nitrogen at position 1 and the other is the nitrogen of the piperazinyl group attached directly to the C-7 atom (N-16). The keto oxygen of OFL and NOR will serve as a good electron acceptor. Having both electron donors and acceptor, OFL and NOR may become one of the good donor–acceptor conjugated molecules. Therefore, it can be proposed the ICT in the excited-state for OFL and NOR as shown in Scheme 5 although the aromaticity of the benzene moiety is damaged to a certain degree [5]. This argument can be supported by the large geometry and dipole moment changes due to excitation in aqueous solutions as described previously. So, it can be assumed that the red shift of the emission band of OFL and NOR in AOT micelle originates from the much slower reorganisation of water molecules following this excited-state ICT of the probe molecule.

The OFL or NOR molecules are initially located in far fewer domains. Following absorption, nonequilibrium solvation exists between solute molecule and solvent cage owing to the Franck–Condon principle. Soon, the solvent molecules undergo dipolar reorganisation about the probe molecule to minimise the free energy of the system and the excited-state molecules begin to emit fluorescence [19,77,78]. If the solvent reorganisation process occurs on a time scale similar to the excited-state lifetime of a probe molecule, the emission spectrum will be red-shifted in response to this reorganisation of the solvent cage. When more water is added into the AOT micelle, the interactions between the water and the probe molecule will become more efficient. Thus, it would be expected that emission is observed from the unrelaxed (short wavelength) and relaxed (long wavelength) states at low and high concentrations of water, respectively [5,79–86].

To find clear evidence for ICT, fluorescence anisotropies were measured [5]. Polarisation excitation spectra of OFL, NOR and FLU obtained in dilute vitrified solution at 77 K are shown in Fig. 6. Because the extrinsic causes of depolarisation are absent in this environment, the observed anisotropy values provide a measure of the angle between the absorption and emission dipoles. In CH_3OH, anisotropies of OFL and NOR are small, and these values decrease as the excita-

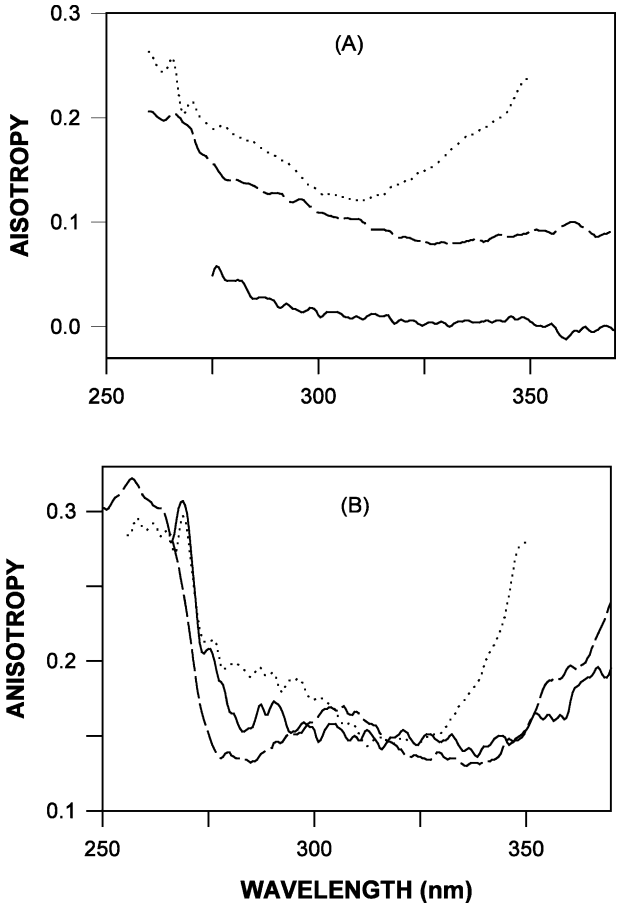

Fig. 6. Steady-state polarisation excitation spectra for 7×10^{-6} M OFL (—), NOR (– – –) and FLU (·····) in (A) methanol, and (B) chloroform solution at $T = 77$ K.

Table 5
Typical impulse response functions recovered from frequency domain measurements for 7×10^{-6} M OFL in 3% (w/v) AOT reverse micelle ($R=2.0$) at 25 °C

Wavelength (nm)	Normalised intensity	τ_1 [a] = 7.45 ns α_1 [b]	τ_2 [a] = 1.09 ns α_2 [b]
400	0.1032	0.093	0.907
420	0.2732	0.220	0.780
440	0.6754	0.289	0.711
480	0.9542	0.370	0.630
505	0.7236	0.557	0.443
535	0.3457	0.635	0.365
560	0.1120	0.625	0.375
			$\lvert\chi\rvert$ [c] = 8.76

[a] Using a global analysis scheme in which the apparent lifetimes are linked throughout the fit.
[b] $|\alpha_1|+|\alpha_2|=1.00$.
[c] The value of reduced $|\chi|$ was calculated based on standard deviations in phase and modulation of 1.76 and 0.013, respectively.

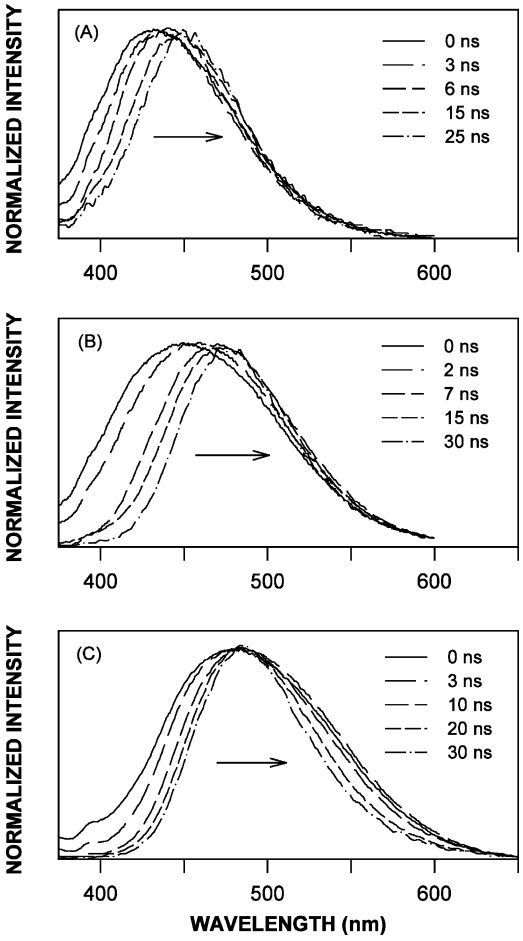

Fig. 7. Normalised time-resolved emission spectra for OFL in AOT reverse micelle at 25 °C. (A) $R=0$; (B) $R=1.98$; (C) $R=9.88$. The arrow indicates the shift of emission band as a function of delay times. The specific time increments are denoted on the individual panels.

tion wavelength increases. This fact suggests that after excitation, ICT will happen quickly before the emission occurs. On the other hand, because the anisotropy of FLU increases rapidly as the excitation wavelength is approached to the long wavelength edge of the absorption band, such charge transfer process will not occur significantly. In $CHCl_3$, the anisotropy increases rapidly as the excitation wavelength moves to the long wavelength side for all OFL, NOR and FLU. Therefore, such excited-state ICT will not occur effectively in $CHCl_3$. So, the polar environment accelerates this excited-state process.

To understand the fluorescence properties of OFL in AOT micelle in more detail, time-resolved fluorescence data were obtained by phase-modulation method [5]. The data were fit more accurately by double-exponential decay model. Table 5 compiles a typical set of recovered apparent lifetimes and preexponential factors. As the emission contour is crossed toward the red edge of the spectrum, it is shown that the portion of the long lifetime component increases and that of the short lifetime component decreases gradually.

Fig. 7 shows the time-resolved fluorescence emission spectra of OFL in AOT reverse micelles as a function of delay time at various amount of added water. These results clearly exhibit the gradual red shift of the emission band as a function of delay time. Also, the time scale for the spectral evolution depends critically on the amount of water within the AOT micelle. Also, the spectra become narrower when the delay time increases. Because emission and solvent relaxation occur at comparable rates, emission will occur from both the unrelaxed and relaxed states, and from a variety of partially relaxed states. As a result, the composite emission displays a broader spectral distribution. As the delay time increases, more fully relaxed emission will appear. So, the red shift and narrower bandwidth of emission spectra can be observed as a function of time.

Several investigators observed a subnanosecond water relaxation component in AOT reverse micelle in addition to the subpicosecond and picosecond components [19,24,25,87]. The faster component is attributed to the solvation dynamics of the inner free water molecules and the slower component is ascribed to the water molecules that interact with the micellar interface. Because of the strong interactions between water and AOT headgroups, unusually slow nanosecond water relaxation can be observed in the AOT micelles.

5.3. Reverse solvatochromism

In many cases, the formation of the charge transfer state is accompanied by an isomerisation reaction in which the donor moiety twists with respect to the acceptor [88–90]. Compounds exhibiting these features are called as twisted intramolecular charge transfer (TICT) molecules. So, OFL and NOR can be regarded

as TICT molecules. The fluorescence spectrum of a TICT molecule will generally exhibit strong solvatochromaticity, which is attributed to the presence of two or more fluorescence isomers of the molecule, the one being in the so-called locally excited configuration, and the others being the charge transfer configurations as shown in AOT reverse micelle.

The steady-state spectroscopic data for OFL in binary mixed solvents are presented in Table 6. In both H_2O–CH_3OH and H_2O–CH_3CN mixed solvents, the fluorescence spectra of this molecule change similar way as a function of solvent composition. The quantum yields of OFL (or NOR) decrease to very small values quickly when the composition of water become less than 12% (w/w). The emission spectra of OFL and NOR displayed the unusual property of reverse solvatochromism. A bathochromic shift occurs from 100% to more than $\sim$55% (w/w) H_2O in both H_2O–CH_3OH and H_2O–CH_3CN mixed solvents, but a hypsochromic shift begins to occur as the composition of water become less than $\sim$55% (w/w).

To investigate the reverse solvatochromism and TICT mechanism of OFL and NOR accurately, the steady-state absorption and fluorescence data were examined by the Lippert–Mataga analysis [91,92]. Within a dielectric continuum approximation of the solvents, the steady-state Stokes' shift can be related to the dipole moment change ($\Delta\mu$) of the probe molecule upon excitation according to the following equation:

$$\Delta\nu = \nu_a - \nu_f = \frac{2(\Delta\mu)^2}{hca^3}\left[\frac{\varepsilon-1}{2\varepsilon+1} - \frac{n^2-1}{2n^2+1}\right] = \frac{2(\Delta\mu)^2}{hca^3}F \quad (1)$$

In the above equation, h is Planck's constant, c is the speed of light, and a is the radius of the cavity in which the solute resides. ν_a and ν_f are the maximum (in cm^{-1}) of the absorption and emission spectra, respectively; ε and n are the dielectric constant and index of refraction of the solvent, respectively. Lippert–Mataga analysis in various mixed solvents is shown in Fig. 8. OFL and NOR exhibit clear reverse solvatochromism in both mixed solvents. The change of dipole moment due to excitation depends strongly upon the solvent composition in both mixed solvent systems because the highly polar environment produced by water will accelerate the excited-state ICT. Also, for FLU, any specific solvent–solute interactions are not observed significantly [92]. In lowest excited-state, OFL and NOR are present mainly as molecular form, $S_1(M)$, in organic solvents or charge transferred zwitterionic form, $S_1(CT)$, in water

Table 6
Stokes' shifts and quantum yields of OFL and solvent parameters of various binary solvent mixtures

H_2O [a] (%)	ν_a (cm^{-1}) [b]	ν_f (cm^{-1}) [b]	$\Delta\nu$ (cm^{-1}) [c]	F [d]	ϕ [e,f]	π^* [g]	α [h]
H_2O–CH_3OH mixtures							
100	30 043	21 089	8954	0.320	0.199	1.14	1.13
96.0	30 216	20 231	9985	0.320	0.185	1.13	1.13
91.9	30 230	20 072	10 158	0.319	0.183	1.11	1.12
79.1	30 288	20 220	10 068	0.319	0.166	1.07	1.11
55.8	30 326	19 947	10 379	0.317	0.197	0.97	1.08
29.6	30 483	20 011	10 472	0.314	0.156	0.83	1.04
12.3	30 581	20 211	10 370	0.311	0.066	0.71	1.01
6.2	30 514	20 381	10 133	0.310	0.025	0.66	1.00
0	30 652	20 784	9868	0.308	0.007[f]	0.60	0.98
H_2O–CH_3CN mixtures							
100	30 043	21 089	8954	0.320	0.199	1.14	1.13
96.0	30 203	20 322	9881	0.320	0.194	1.12	1.09
92.0	30 285	20 110	10 175	0.319	0.199	1.11	1.05
79.2	30 338	19 930	10 408	0.317	0.202	1.05	0.96
56.0	30 442	19 725	10 717	0.314	0.257	0.95	0.90
29.8	30 504	19 768	10 736	0.310	0.255	0.84	0.89
12.4	30 565	19 968	10 597	0.307	0.214	0.78	0.77 [i]
6.3	30 559	20 153	10 406	0.306	0.070	0.77	0.58 [i]
0	30 597	20 320	10 277	0.305	0.004[f]	0.75	0.19

[a] Wt.% of H_2O in H_2O–CH_3OH or H_2O–CH_3CN mixtures.
[b] Energy of absorption (ν_a) or fluorescence centre of gravity (ν_f). Uncertainty is ± 60 cm^{-1}.
[c] $\Delta\nu = \nu_a - \nu_f$.
[d] Dielectric function F defined in Eq. (1).
[e] Fluorescence quantum yields. Uncertainty is $\leq$6% except as noted.
[f] Uncertainty is $\leq$15% owing to very low fluorescence intensity.
[g] Index of solvent dipolarity/polarisability.
[h] Solvent hydrogen-bond donor acidity.
[i] These values have relatively large uncertainty ($\leq$5%) owing to the abrupt change as the increase of CH_3CN in mixtures.

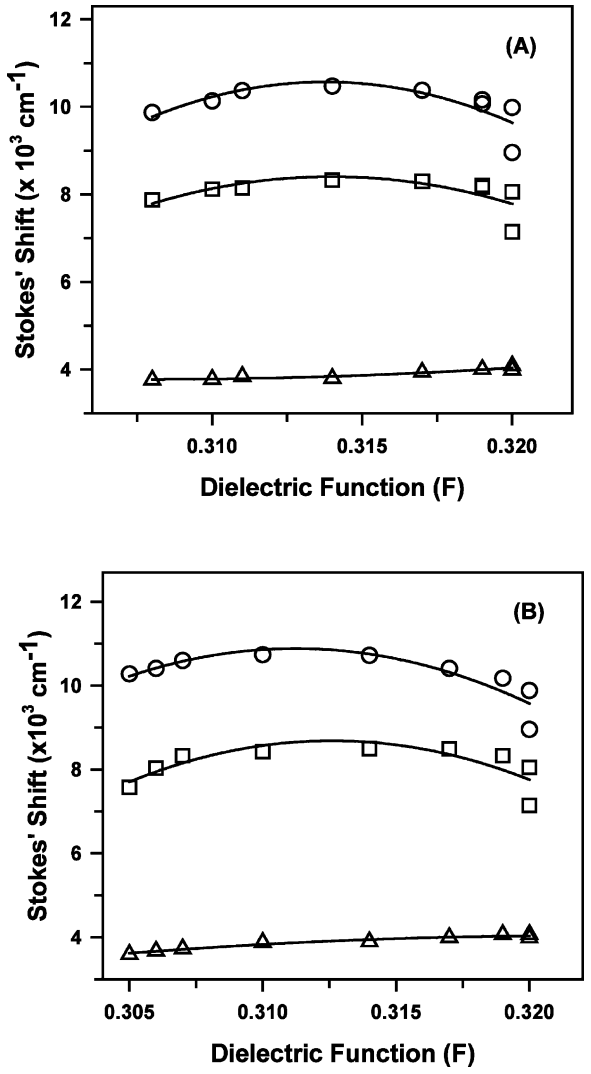

Fig. 8. Lippert–Mataga plot for OFL (○), NOR (□), and FLU (△) in H_2O–CH_3OH, (A), and H_2O–CH_3CN, (B), mixed solvents. The steady-state Stokes' shift is plotted against the dielectric function (F) defined in Eq. (1). The solid lines are the best polynomial regression fits to the data.

(see Scheme 6) [4,5,12]. However, in hydro-organic mixtures, the molecular structure of the OFL (or NOR) will lie somewhere between that of both mesomeric structures, S_1(M), and S_1(CT), depending on the solvatochromic parameters of mixed solvents [12,73,93,94]. Therefore, it may be assumed that the S_1(PM) and S_1(PZ), which exist in intermediate meropolymethine state, are formed by partial ICT. The protolytic equilibrium between S_1(M) and S_1(Z), and S_1(PM) and S_1(PZ) may be present. Also, it can be suggested that S_1(PM) and S_1(PZ) may have the longest wavelength emission band. Water stabilise the form S_1(CT), and organic solvents, the form S_1(M). Hydro-organic mixtures stabilise the low-energy polymethine form, S_1(PM) and S_1(PZ). Thus, hypsochromic shifts can occur in either water or organic media.

In AOT reverse micelle, only one ICT state, S_1(ICT), was suggested because reverse solvatochromism was not observed as a function of added water [5]. The polarity of the interior of AOT reverse micelle is about the same as that of the hydro-organic mixed solvents. Therefore, it can be assumed that the electrical and geometrical structure of the S_1(ICT) in AOT micelle may have the similar to that of the S_1(PZ) or S_1(PM) in hydro-organic mixed solvents.

5.4. Theoretical treatment for the change of molecular structure in the excited-state

To support the mechanism of TICT process of OFL or NOR, the bond length changes of OFL due to excitation are calculated in gas and aqueous phase as shown in Table 7. [5,12]. In aqueous phase, the bonds *b*, *e*, *g* and *i* are greatly shortened and the bonds *c*, *d*, *f* and *h* are lengthened upon excitation. In gas phase, these kinds of bond length changes are not exhibited. The electron density of the N-16 atom decreases and the electron density of the C-7 increases greatly due to excitation in aqueous phase (data are not shown). Also, the negative charges of position 2, 3, 4 and 10 carbons and the carboxylic and keto group atoms increase slightly. Therefore, this theoretical treatment of this molecule is consistent with the suggested mechanism of excited-state ICT.

In aqueous solution, the dihedral angles (CCNC) of molecular moiety around C-7 and N-16 are 145.3 and 168.0° at the ground and excited-state, respectively [5,12]. Because the dihedral angles of perfect sp^3 and sp^2 hybridisation are 120.0 and 180.0°, respectively, the bond between C-7 and N-16 will be close to single bond at the ground state but this bond will have more double bond character at the excited-state. To change from S_1(Z) to S_1(PZ) and S_1(CT), potential energy barrier should be crossed because the molecular moiety around C-7 and N-16 does not form a single plane and the bond between this carbon and nitrogen atom will have more sp^2 character and geometry as the chemical species is changed to S_1(PZ) and S_1(CT). Owing to these energy barriers, each chemical species in suitable environment will be present in relatively stable state. So, reverse solvatochromism in the fluorescence spectrum can be observed. In gas phase, OFL will be present as molecular form and the dihedral angles (CCNC) of the molecular moiety around C-7 and N-16 are 141.2 and 179.6° at the ground and excited-state, respectively [5,12]. So, the quinoline moiety and N-16 form nearly single plane and the chemical bond between C-7 and N-16 have nearly perfect sp^2 character at the S_1 state. The lone pair electrons of N-16 are effectively delocalised over the aromatic ring. Although several chemi-

cal species may possibly be present at the S_1 state, there will be essentially no energy barrier among these species. So, only single species will be found at the S_1 state. It can be assumed that the excited-state OFL is present as a hybrid structure in gas phase, which may somewhat be similar to S_1(PM) in Scheme 6.

5.5. Radiative and non-radiative rate constants

To study the effect of solvent on the excited-state dynamics further, the radiative (k_r) and non-radiative rate constants (k_{nr}) were obtained [12,91]. In Table 8, lifetimes and the radiative and non-radiative rate constants of antibiotics, are shown [12].

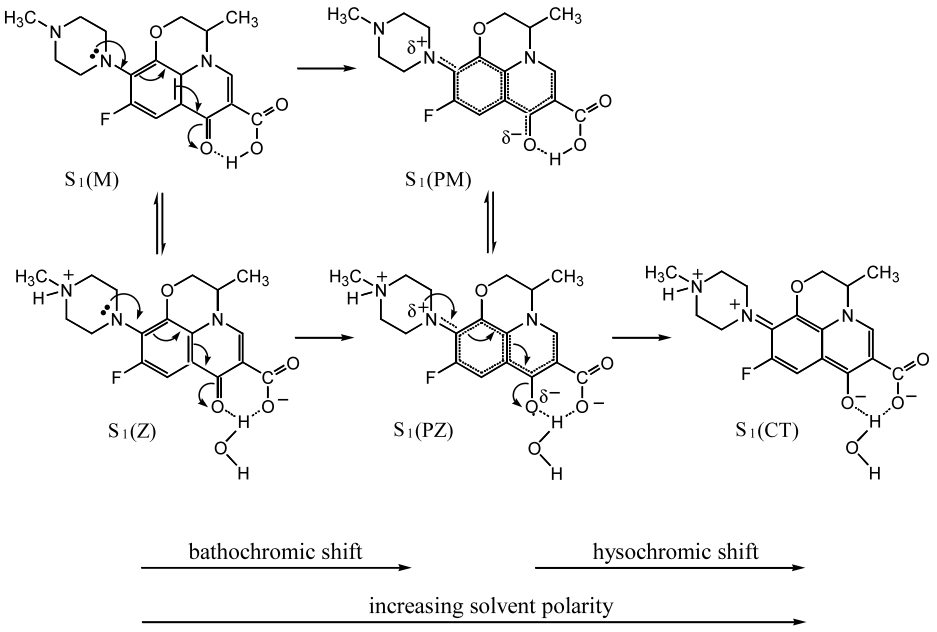

Scheme 6.

Table 7
Bond length changes (Å) of OFL upon excitation in gas and aqueous phase obtained by AM1 COSMO model

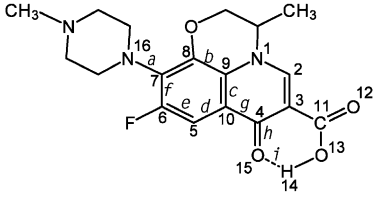

Chemical bond	Bond length in gas phase		Bond length in aqueous phase		Δr_1[a]	Δr_2[a]	Δr_3[b]	Δr_4[c]
	S_0	S_1	S_0	S_1				
A	1.406	1.375	1.409	1.412	−0.031	+0.003	+0.003	+0.037
B	1.422	1.426	1.419	1.398	+0.004	−0.021	−0.003	−0.028
C	1.411	1.439	1.415	1.436	+0.028	+0.021	+0.004	−0.003
D	1.398	1.383	1.396	1.419	−0.015	+0.023	−0.002	+0.036
E	1.395	1.404	1.397	1.375	+0.009	−0.022	+0.002	−0.029
F	1.439	1.476	1.432	1.446	+0.037	+0.014	+0.007	−0.030
G	1.475	1.474	1.471	1.439	−0.001	−0.032	−0.004	−0.035
H	1.245	1.248	1.256	1.267	+0.003	+0.011	+0.011	+0.019
I	1.999	1.999	1.986	1.953	0	−0.033	−0.013	−0.046

[a] Δr_1, Δr_2: The change of bond length upon excitation in gas and aqueous phase respectively.
[b] Δr_3: Bond length difference between gas and aqueous phase in S_0 state.
[c] Δr_4 : Bond length difference between gas and aqueous phase in S_1 state.

Table 8
Fluorescence lifetimes and calculated radiative and non-radiative rate constant for antibiotics

H_2O [a] (%)	OFL			NOR			FLU		
	τ [b] (ns)	k_r (10^7 s^{-1})	k_{nr} (10^8 s^{-1})	τ [b] (ns)	k_r (10^7 s^{-1})	k_{nr} (10^8 s^{-1})	τ [b] (ns)	k_r (10^7 s^{-1})	k_{nr} (10^8 s^{-1})
H_2O–CH_3OH mixtures									
100	5.86	3.40	1.37	2.30	6.48	3.70	0.73	4.66	13.2
96.0	7.38	2.51	1.10	1.68	9.23	5.03	1.02	3.82	9.42
91.9	5.94	3.08	1.38	1.67	9.04	5.08	0.99	4.24	9.68
79.1	7.27	2.28	1.15	1.68	8.99	5.05	0.98	4.59	9.75
55.8	10.5	1.88	0.76	1.73	7.46	5.03	0.93	4.62	10.3
29.6	11.4	1.37	0.74	1.95	5.90	4.54	0.62	6.61	15.5
12.3	11.4	0.58	0.82	1.99	3.72	4.65	0.54	7.59	17.8
6.2	11.4	0.22	0.86	2.40	2.92	3.88	0.52	7.89	18.4
0	12.5	0.06	0.79	2.56	0.78	3.83	0.82	4.63	11.7
H_2O–CH_3CN mixtures									
100	5.86	3.40	1.37	2.30	6.48	3.70	0.73	4.66	13.2
96.0	6.98	2.78	1.16	1.75	8.23	4.89	0.79	4.68	12.2
92.0	5.47	3.64	1.46	1.61	8.39	5.37	0.74	4.60	13.1
79.2	7.43	2.72	1.07	1.94	7.63	4.39	0.66	5.15	14.6
56.0	6.68	3.85	1.11	2.26	8.05	3.62	0.46	6.74	21.1
29.8	11.5	2.22	0.65	2.47	8.42	3.21	0.45	6.22	21.6
12.4	12.0	1.78	0.66	2.96	8.62	2.52	0.40	6.25	24.4
6.3	12.7	0.55	0.73	3.14	4.33	2.75	0.62	4.36	15.7
0	13.7	0.03	0.73	3.05	0.16	3.26	0.76	3.29	12.8

[a] Wt.% of H_2O in H_2O–CH_3OH or H_2O–CH_3CN mixtures.
[b] Fluorescence lifetimes. Uncertainty is less than $\pm 8\%$.

The dependence of k_{nr} on solvent polarity, as measured by the π^* scale was examined as shown in Fig. 9 [12,91,95,96]. As the solvent polarity increases in both hydro-organic mixed solvents, the k_{nr} of OFL and NOR increases (approximatively), but the k_{nr} of FLU increases at first and begins to decrease when the amount of water is more than ~ 10 or $\sim 25\%$. The possible role of specific hydrogen bonding interactions on the non-radiative decay rate can be studied by examining the dependence of k_{nr} on the α scale as shown in Fig. 10 [12,91,95,96]. In both H_2O–CH_3OH and H_2O–CH_3CN solvents, the changes of k_{nr} as a function of α or π^* are roughly the same for all OFL, NOR and FLU. So, it can be suggested that the influence of bulk dielectric effect of the medium is more important than that of the specific hydrogen bonding interactions as described by the Lippert–Mataga analysis previously.

Usually, the non-radiative rate constants are expressed in terms of an energy gap law

$$k_{nr} \propto \exp(-\alpha \Delta E) \quad (2)$$

where ΔE is the energy gap between the ground and excited electronic states [91]. When the water composition begins to increase in mixed solvents, ΔE decreases owing to the red shift of emission band and the k_{nr} of OFL (or NOR) increases. However, when the amount of water in both mixed solvents exceeds $\sim 55\%$ (w/w), hypsochromic shift of emission band occurs. So, under this circumstance, other reasons should be examined.

Zwitterionic form of OFL (or NOR) has both positive and negative charge. The S_1(PZ) form in Scheme 6 has extra charge at 4-keto oxygen and N-16. The S_1(CT) form has further extra charge at these atoms. The principal species of the excited-state OFL (or NOR) in mixed solvent is changed as shown in Scheme 6. Therefore, as the water composition increases, the intermolecular interaction between H_2O and solute becomes stronger, which may lead to an increase in the non-radiative relaxation rates from S_1 to S_o [12,91,97,98]. So, it can be assumed that the k_{nr} of these species may increase as the following order: S_1(M), S_1(Z), S_1(PZ) and S_1(CT). The k_{nr} of S_1(PM) may be similar to that of S_1(Z).

When the water begins to mix in CH_3OH or CH_3CN, the non-radiative relaxation rate of FLU will increase because of the stronger intermolecular interaction between H_2O and the polar groups or atoms of FLU. As the composition of water increases in both mixed solvents, the dissociation of 3-carboxylic acid group will begin to occur [5,11,12]. According to the Fig. 9, it can be assumed that the k_{nr} of FLU anions is slower than that of FLU molecules in this environment. Contrary to the H_2O–CH_3OH, H_2O–CH_3CN mixtures show various structural features according to the composition [4,12,99–103]. Therefore, the change of k_{nr} in H_2O–CH_3CN is slightly different from that in H_2O–CH_3OH solvents.

The effect of solvent on the radiative decay rate was also studied [12]. According to the Strickler–Berg relation [12,91,104], the k_r will be proportional to the molar absorptivity at absorption maximum (ε_{max}) and the cube of the emission centre of gravity (ν_f) if the absorption bands of the lowest energy transition are assumed to be Gaussian. In both H_2O–CH_3OH and H_2O–CH_3CN solvent systems, (ε_{max}) $(\nu_f)^3$ of OFL, NOR and FLU is nearly constant as a function of solvent composition. As shown in Table 8 and Figs. 11 and 12, the k_r of OFL and NOR show dramatic change as a function of solvatochromic parameters in both mixed solvent systems, but this rate of FLU does not exhibit any significant variations. Therefore, the k_r of OFL and NOR do not follow the Strickler–Berg relation. This observation may become another evidence that OFL and NOR are the TICT molecules in highly polar and protic environments. Since the change of k_r as a function of π^* or α is similar to each other in both hydro-organic mixed solvents, the bulk dielectric effect

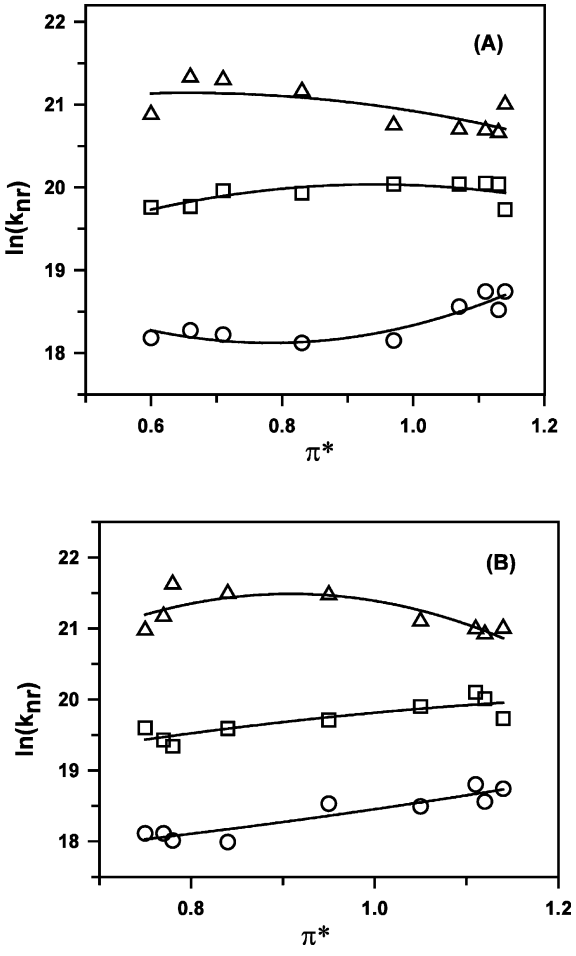

Fig. 9. Logarithm of the non-radiative rate constant, k_{nr}, plotted as a function of the solvent polarity parameter, π^*, in H_2O–CH_3OH, (A), and H_2O–CH_3CN, (B), mixed solvents: OFL (○), NOR (□), FLU (△). The solid lines are the best polynomial regression fits to the data.

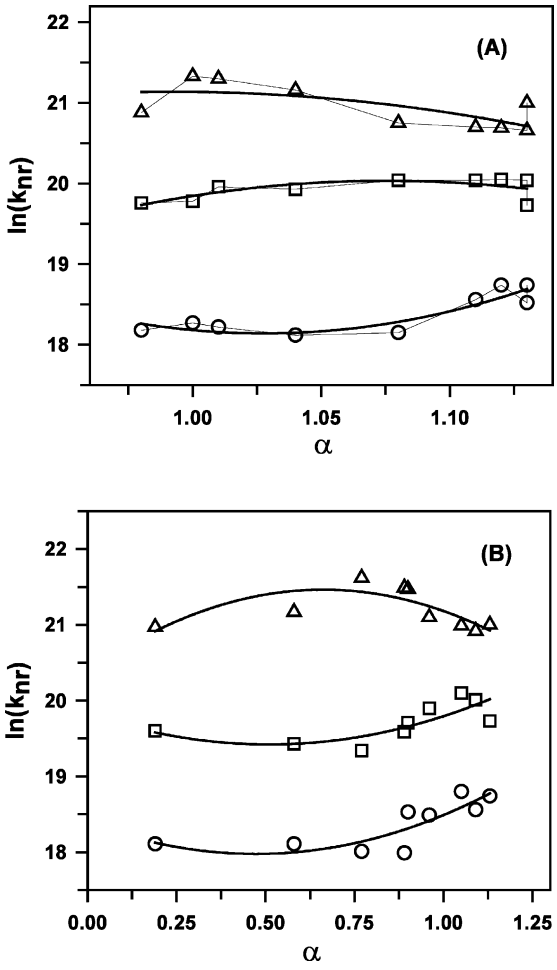

Fig. 10. Logarithm of the non-radiative rate constant, k_{nr}, plotted as a function of the hydrogen-bond donating strength, α in H_2O–CH_3OH, (A), and H_2O–CH_3CN, (B), mixed solvents: OFL (○), NOR (□), FLU (△). The solid lines are the best polynomial regression fits to the data.

of solvent overwhelm the specific hydrogen bonding interaction for all solute molecules. Therefore, the radiative decay rate may be primarily determined by the question; which is the principal species in certain environment? The k_r of each species may increase as the following order: S_1(M), S_1(Z) and S_1(PM), S_1(PZ), and S_1(CT). This situation is the same as the change of k_{nr}. So, the k_r in both hydro-organic mixed solvents increases rapidly as a function of water composition. However, in acetonitrile rich region of H_2O–CH_3CN mixed solvents, the change of k_r is much more dramatic. This observation may be explained by the fact that the solute will be preferentially solvated by 'free' water molecules and ICT will effectively be initiated at the early time when the amount of water begins to increase [4,12]. In the water-rich environment of both H_2O–CH_3OH and H_2O–CH_3CN mixed solvents, the k_r does not increase significantly as a function of water composition because most of the OFL (or NOR) will be present as S_1(CT). In H_2O–CH_3CN solvents, when

the water composition is greater than ~15% (w/w), the increase of preferential solvation by water does not significantly influence the excited-state chemical process any more. Furthermore, when the amount of water increases more than 70%, there will be preferential solvation by acetonitrile owing to the strong self-association interactions among the water molecules [4,12].

6. Conclusion

The molecular structure of quinolone antibiotics was modified by introduction of fluorine atom at position 6 and piperazinyl group at position 7. This kind of drugs such as OFL and NOR exhibits greatly improved antibacterial activity. Because OFL and NOR are good TICT molecules in the excited-state, they exhibits characteristic spectroscopic properties. These chemical properties of TICT molecules may be related to the significant improvement of antibacterial activity compared with the quinolones, which does not have piperazinyl group. Therefore, the photochemical properties of these TICT quinolone molecules are intensively examined in biological mimetic systems.

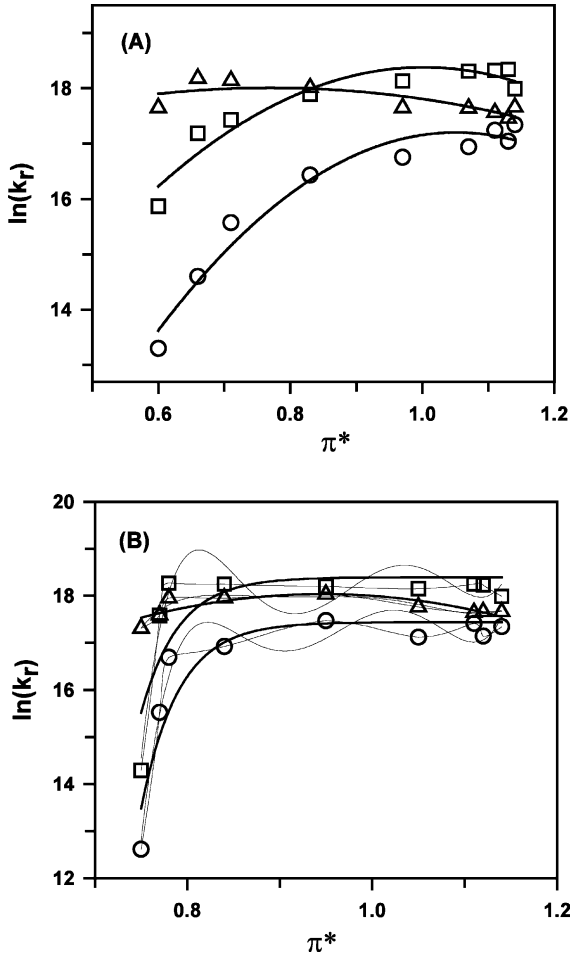

Fig. 11. Logarithm of the radiative rate constant, k_r, plotted as a function of the solvent polarity parameter, π^*, in H_2O–CH_3OH, (A), and H_2O–CH_3CN, (B), mixed solvents: OFL (○), NOR (□), FLU (△). (A) The solid lines are the best polynomial regression fits to the data. (B) The solid lines are not exactly the best fits to the data but suggest the general trend for each antibiotics.

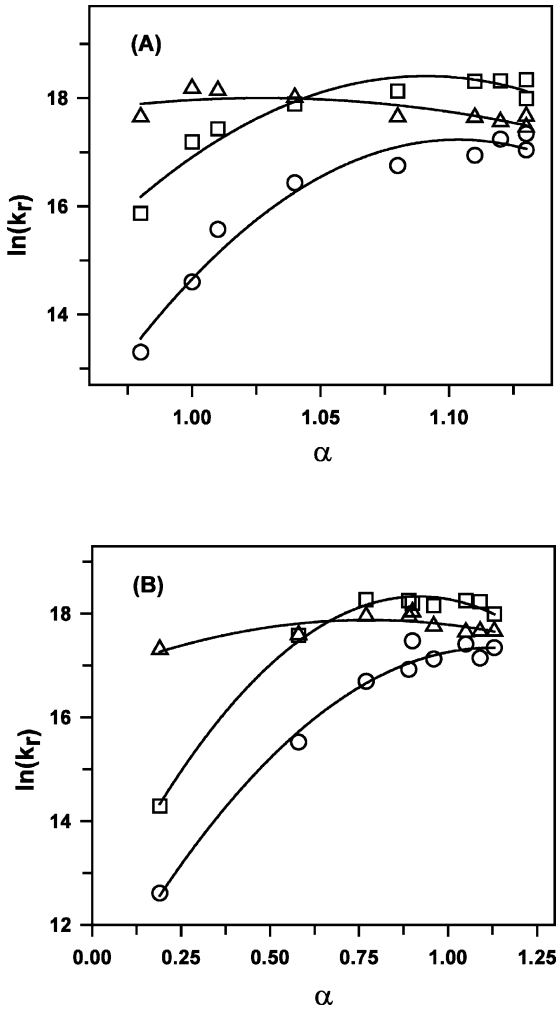

Fig. 12. Logarithm of the radiative rate constant, k_r, plotted as a function of the hydrogen-bond donating strength, α, in H_2O–CH_3OH, (A), and H_2O–CH_3CN, (B), mixed solvents: OFL (○), NOR (□), FLU (△). The solid lines are the best polynomial regression fits to the data.

The excited-state ICT of OFL and NOR was first observed in AOT micelle. Because this chemical process is accelerated by water, OFL and NOR are present as molecular form in CH_3OH or CH_3CN, but these molecules are present mainly as charge transferred zwitterionic form in aqueous solution. In hydro-organic mixtures, OFL and NOR exist in intermediate meropolymethine state, which will have the longest wavelength emission. Therefore, in Lippert–Mataga analysis of the steady-state fluorescence data, OFL and NOR exhibit a reverse solvatochromism in both H_2O–CH_3OH and H_2O–CH_3CN mixed solvents. The change of k_{nr} and k_r as a function of π^* and α scale for mixed

solvents can also be explained by this excited-state ICT. The physicochemical properties of OFL and NOR depends more strongly upon the bulk dielectric effect of solvents relative to the specific hydrogen bonding interactions.

To be brief, two kinds of photochemical reactions have been observed. For NAL, the decarboxylation at position 3 is observed. For the 6,8-difluoro derivatives such as LOM and FLE, effective defluorination at position 8 as fluoride ion is exhibited. For 6-fluoro derivatives such as NOR and ENO, less effective C–F bond cleavage is observed. The fragmentation of this C–F bond is a heterolytic process. Also, the reactivity of the singlet state appears to be related to the ICT character of this state. This reaction would appear to be of interest, since there are very few examples of cleavage of this strong bond. Also, this photodecomposition may partly explain the photosensitivity mechanism of fluoroquinolones. So, all of these studies will provide further insight into antibacterial activity and the photosensitivity mechanism of quinolone antibiotics.

References

[1] P.C. Appelbaum, P.A. Hunter, Int. J. Antimicrob. Agents 16 (2000) 5–15.
[2] Y. Mizuki, I. Fujiwara, T. Yamaguchi, J. Antimicrob. Chemother. 37 (Suppl. A) (1996) 41–55.
[3] P. Ball, J. Antimicrob. Chemother. 46 (2000) 17–24 Topic T1.
[4] V. Snaz-Nebot, I. Valls, D. Barbero, J. Barbosa, Acta Chem. Scand. 51 (1997) 896–903.
[5] H.R. Park, H.C. Lee, T.H. Kim, J.K. Lee, K. Yang, K.M. Bark, Photochem. Photobiol. 71 (2000) 281–293.
[6] M. Neuman, Clin. Pharmacokinet. 14 (1988) 96–121.
[7] X. Yu, G.L. Zipp, W.R. Davidson, Pharm. Res. 11 (1994) 522–527.
[8] K. Takacs-Novak, B. Noszal, I. Hermecz, G. Kereszturi, B. Podanyi, G. Szasz, J. Pharm. Sci. 79 (1990) 1023–1028.
[9] J. Barbosa, R. Bergés, I. Toro, V. Sanz-Nebot, Int. J. Pharm. 149 (1997) 213–225.
[10] J.T. Smith, C.S. Lewin, in: V.T. Andriole (Ed.), The Quinolones, Academic Press, New York, USA, 1988, pp. 23–82.
[11] H.R. Park, K.Y. Chung, H.C. Lee, J.K. Lee, K.M. Bark, Bull. Korean Chem. Soc. 21 (2000) 849–854.
[12] H.R. Park, C.H. Oh, H.C. Lee, J.K. Lee, K. Yang, K.M. Bark, Photochem. Photobiol., in press.
[13] J.S. Kang, T.H. Kim, K.B. Park, B.H. Chung, J.I. Youn, Photodermatol. Photoimmunol. Photomed. 9 (1993) 159–161.
[14] J. Barbosa, G. Fonrodona, I. Marqués, V. Sanz-Nebot, I. Toro, Anal. Chim. Acta 351 (1997) 397–405.
[15] J. Barbosa, R. Bergés, I. Toro, V. Sanz-Nebot, Talanta 44 (1997) 1271–1283.
[16] P. Bilski, L.J. Martinez, E.B. Koker, C.F. Chignell, Photochem. Photobiol. 68 (1998) 20–24.
[17] M. Wong, J.K. Thomas, M. Gratzel, J. Am. Chem. Soc. 98 (1976) 2391–2397.
[18] F.M. Menger, G. Saito, J. Am. Chem. Soc. 100 (1977) 4376–4379.
[19] J. Zhang, F.V. Bright, J. Phys. Chem. 95 (1991) 7900–7907.
[20] T.K. Jain, M. Varshney, A. Maitra, J. Phys. Chem. 93 (1989) 7409–7416.
[21] K.K. Karukstis, A.A. Frazier, D.S. Martula, J.A. Whiles, J. Phys. Chem. 100 (1996) 11133–11138.
[22] F. Grieser, C.J. Drummond, J. Phys. Chem. 92 (1988) 5580–5593.
[23] A. D'Aprano, A. Lizzio, V. Turco Liveri, F. Aliotta, C. Vasi, P. Migliardo, J. Phys. Chem. 92 (1988) 4436–4439.
[24] R.E. Riter, E.P. Undiks, N.E. Levinger, J. Am. Chem. Soc. 120 (1998) 6062–6067.
[25] R.E. Riter, D.M. Willard, N.E. Levinger, J. Phys. Chem. B 102 (1998) 2705–2714.
[26] P.D.I. Fletcher, A.M. Howe, B.H. Robinson, J. Chem. Soc. Faraday Trans. I 83 (1987) 985–1006.
[27] P. Grigolini, M. Maestro, Chem. Phys. Lett. 127 (1986) 248–252.
[28] V. Kim, G.Y. Frolov, V.I. Ermakov, S.E. Pak, Kolloidn. Zh. 49 (1987) 1067–1069.
[29] B.G. Katzung, Basic and Clinical Pharmacology, 8th ed., Lange Medical Books/McGraw-Hill, New York, 2001, pp. 797–802.
[30] H. Koga, A. Itoh, S. Murayama, S. Suzue, T.X. Irikura, J. Med. Chem. 23 (1980) 1358–1363.
[31] J.F. Gerster, Ger. Pat. 2, 264 (1973), 163.
[32] Y.W. Sun, E.P. Heo, Y.H. Cho, K.M. Bark, T.J. Yoon, T.H. Kim, Photodermatol. Photoimmunol. Photomed. 17 (2001) 172–177.
[33] J. Ferguson, Photochem. Photobiol. 62 (1995) 954–958.
[34] A.R. Saniabaldi, K. Wada, K. Umemura, S. Sakuma, M. Nakashima, J. Photochem. Photobiol. B: Biol. 33 (1996) 137–142.
[35] N. Umezawa, K. Arakane, A. Ryu, S. Mashiko, M. Hirobe, T. Nagano, Arch. Biochem. Biophys. 342 (1997) 275–281.
[36] G. Ouedraogo, P. Morlière, M. Bazin, R. Santus, B. Kratzer, M.A. Miranda, J.V. Castell, Photochem. Photobiol. 70 (1999) 123–129.
[37] K. Shimoda, M. Kato, Arch. Toxicol. 72 (1998) 251–256.
[38] J.A. Parrish, L.T. Chylack, M.E. Woehler, H.M. Cheng, M.A. Pathak, W.L. Morison, J. Krugler, W.F. Nelson, J. Invest. Dermatol. 73 (1979) 250–255.
[39] R.S. Stern, Toxicol. Lett. 102–103 (1998) 389–392.
[40] R.S. Stern, N. Laird, Cancer 73 (1994) 2759–2764.
[41] G. Klekak, F. Urbach, H. Urwyler, J. Photochem. Photobiol. B: Biol. 37 (1997) 174–181.
[42] M. Mäkinen, P.D. Forbes, F. Steinbäck, J. Photochem. Photobiol. B: Biol. 37 (1997) 182–187.
[43] Y. Tokura, T. Nishijima, H. Yagi, F. Furukawa, M. Takigawa, Photochem. Photobiol. 64 (1996) 838–844.
[44] T. Horio, H. Miyauchi, Y. Asada, Y. Aoki, M. Harada, J. Dermatol. Sci. 7 (1994) 130–135.
[45] J.E. Rosen, D. Chen, A.K. Prahalad, T.E. Spratt, G. Schluter, G.M. Williams, Toxicol. Appl. Pharmacol. 145 (1997) 381–387.
[46] N. Detzer, B. Huber, Tetrahedron 31 (1975) 1937–1941.
[47] E. Fernández, A.M. Cárdenas, J. Photochem. Photobiol. B: Biol. 4 (1990) 329–333.
[48] L.J. Martinez, G. Li, C.F. Chignell, Photochem. Photobiol. 65 (1997) 599–602.
[49] E. Fasani, F.F. Barberis Negra, M. Mella, S. Monti, A. Albini, J. Org. Chem. 64 (1999) 5388–5395.
[50] E. Fasani, M. Mella, D. Caccia, S. Tassi, M. Fagnoni, A. Albini, Chem. Commun. (1997), 1329–1330.
[51] E. Fasani, A. Profumo, A. Albini, Photochem. Photobiol. 68 (1998) 666–674.
[52] S. Monti, S. Sortino, E. Fasani, A. Albini, Chem. Eur. J. 7 (2001) 2185–2196.
[53] E. Fasani, M. Mella, S. Monti, A. Albini, Eur. J. Org. Chem. (2001), 391–397.

[54] G. Vermeersch, J.C. Ronfard-Haret, M. Bazin, V. Carillet, P. Morliere, R. Santus, Photochem. Photobiol. 54 (1991) 661–666.
[55] P. Dayhaw-Barker, G.T. Truscott, Photochem. Photobiol. 47 (1988) 765–767.
[56] M. Gellert, K. Mizuuchi, M.O.O. Dea, T. Itoh, J.I. Tomizawa, Proc. Natl. Acad. Sci. USA 74 (1977) 4772–4776.
[57] D.E. Moore, V.J. Hemmens, H. Yip, Photochem. Photobiol. 39 (1984) 57–61.
[58] K. Timmers, R. Sternglanz, Bioinorg. Chem. 9 (1978) 145–155.
[59] D.L. Ross, C.M. Riley, Int. J. Pharm. 83 (1992) 267–272.
[60] H.B. Hetzer, R.A. Robinson, R.G. Bates, J. Phys. Chem. 72 (1968) 2081–2086.
[61] O. Enea, K. Honugbossa, G. Berthon, Electrochim. Acta 17 (1972) 1585–1594.
[62] L. Martinez, P. Bilski, C.F. Chignell, Photochem. Photobiol. 64 (1996) 911–917.
[63] G. Palu, S. Valisena, G. Ciarrocchi, B. Gatto, M. Palumbo, Proc. Natl. Acad. Sci. USA 89 (1992) 9671–9675.
[64] S. Bazile-Pham Khac, N.J. Moreau, J. Chrom. A 668 (1994) 241–247.
[65] J. Slater, A. Mildvan, L. Loeb, Biochem. Biophys. Res. Commun. 44 (1971) 37–43.
[66] C. Springgate, A. Mildvan, R. Abramson, J. Engle, L. Loeb, J. Biol. Chem. 248 (1973) 5987–5993.
[67] P. Valenzuela, R. Morris, A. Faras, W. Levinson, W. Rutter, Biochem. Biophys. Res. Commun. 53 (1973) 1036–1041.
[68] A.J.G. Bailey, A. Cole, J. Goodfield, P.M. May, M.E. Dreyfuss, J.M. Midgley, D.R. Williams, Int. J. Pharm. 22 (1984) 283–290.
[69] J.C. Jimenez Sanchez, J.A. Munoz Leyva, M. Roman Ceba, Anal. Chim. Acta 90 (1977) 223–231.
[70] D.L. Ross, C.M. Riley, Int. J. Pharm. 93 (1993) 121–129.
[71] N.B. Behrens, G.M. Diaz, D.M.L. Goodgame, Inorg. Chim. Acta 125 (1986) 21–26.
[72] D.L. Ross, C.M. Riley, Int. J. Pharm. 87 (1992) 203–213.
[73] G.M. Anstead, K.J. Hwang, J.A. Katzenellenbogen, Photochem. Photobiol. 57 (1993) 616–628.
[74] G. Weber, F.J. Farris, Biochemistry 18 (1979) 3075–3081.
[75] F.G. Prendergast, G.I. Meyer, S.I. Carlson, J.D. Potter, J. Biol. Chem. 258 (1983) 7541–7544.
[76] T.K. De, A. Maitra, Adv. Colloid. Interf. Sci. 59 (1995) 95–193.
[77] J.R. Lakowicz, H. Cherek, Chem. Phys. Lett. 122 (1985) 380–384.
[78] J.R. Lakowicz, E. Gratton, H. Cherek, B.P. Maliwal, G. Laczko, J. Biol. Chem. 259 (1984) 10967–10972.
[79] E.M. Kosower, H.J. Dudiuk, J. Phys. Chem. 82 (1978) 2012–2015.
[80] K.H. Grellman, U. Schmitt, J. Am. Chem. Soc. 104 (1982) 6267–6272.
[81] E.M. Kosower, H. Kanety, H. Dodiuk, G. Striker, T. Jovin, H. Boni, D. Huppert, J. Phys. Chem. 87 (1983) 2479–2484.
[82] G.C. Catena, F.V. Bright, Anal. Chem. 61 (1989) 905–909.
[83] F.V. Bright, G.C. Catena, J. Huang, J. Am. Chem. Soc. 112 (1990) 1343–1346.
[84] J. Huang, F.V. Bright, J. Phys. Chem. 94 (1990) 8457–8463.
[85] T.W. Ebberson, C.A. Ghiron, J. Phys. Chem. 93 (1989) 7139–7143.
[86] E.M. Kosower, J. Am. Chem. Soc. 107 (1985) 1114–1118.
[87] N. Sarkar, K. Das, A. Datta, S. Das, K. Bhattacharyya, J. Phys. Chem. 100 (1996) 10523–10527.
[88] R.D. Schulte, J.F. Kauffman, Appl. Spectros. 49 (1995) 31–39.
[89] W. Rettig, Angew. Chem. 98 (1986) 969–986.
[90] W. Rettig, J. Mol. Struct. 84 (1982) 303–327.
[91] R.S. Moog, N.A. Burozski, M.M. Desai, W.R. Good, C.D. Silvers, P.A. Thompson, J.D. Simon, J. Phys. Chem. 95 (1991) 8466–8473.
[92] J.R. Lakowicz, Principles of Fluorescence Spectroscopy, Plenum Press, New York, 1983, pp. 190–201.
[93] L. Lu, R.J. Lachicotte, T.L. Penner, J. Perlstein, D.G. Whitten, J. Am. Chem. Soc. 121 (1999) 8146–8156.
[94] P. Jacques, J. Phys. Chem. 90 (1986) 5535–5539.
[95] C. Reichardt, Solvents and Solvent Effects in Organic Chemistry, VCH, Weinheim, Germany, 1988, pp. 372–384.
[96] M.J. Kamlet, J.L.M. Abboud, R.W. Taft, Prog. Phys. Org. Chem. 13 (1981) 485–630.
[97] H. Inoue, M. Hida, N. Nakashima, K. Yoshihara, J. Phys. Chem. 86 (1982) 3184–3188.
[98] S.R. Flom, P.F. Barbara, J. Phys. Chem. 89 (1985) 4489–4494.
[99] J. Barbosa, V. Sanz-Nebot, J. Chem. Soc., Faraday Trans. 90 (1994) 3287–3292.
[100] Y. Marcus, Y. Migron, J. Phys. Chem. 95 (1991) 400–406.
[101] H. Kovacs, A. Laaksonen, J. Am. Chem. Soc. 113 (1991) 5596–5605.
[102] O. Budewsky, Foundations of Chemical Analysis, Ellis Horwood, Chichester, 1979.
[103] J.G. Dawber, J. Ward, R.A. Williams, J. Chem. Soc. Faraday Trans. I 84 (1988) 713–727.
[104] S.J. Strickler, R.A. Berg, J. Chem. Phys. 37 (1962) 814–822.